On the Axisymmetric Counterflow Flame Simulations: Is There an Optimal Nozzle Diameter and Separation Distance to Apply Quasi One-Dimensional Theory?

R. F. Johnson, A. C. VanDine, G. L. Esposito & H. K. Chelliah

Taylor & Francis
Taylor & Francis Group

ON THE AXISYMMETRIC COUNTERFLOW FLAME SIMULATIONS: IS THERE AN OPTIMAL NOZZLE DIAMETER AND SEPARATION DISTANCE TO APPLY QUASI ONE-DIMENSIONAL THEORY?

R. F. Johnson, A. C. VanDine, G. L. Esposito, and H. K. Chelliah

Department of Mechanical and Aerospace Engineering, University of Virginia, Charlottesville, Virginia, USA

Two-dimensional axisymmetric numerical analysis of counterflow flames was employed to better understand the applicability of the quasi one-dimensional theory of Seshadri and Williams to flames produced by small diameter convergent nozzles. The computational domain considered included the convergent sections of two opposed nozzles as well as the surrounding inert annular co-flows. For computational efficiency, the fuel-oxidizer system of diluted hydrogen versus air in non-premixed flame mode, with a detailed chemical kinetic model and mixture-averaged transport property description, was considered. With an increase of nozzle diameter from 6.5 mm to larger values (with plug flow velocity profiles at the nozzle exit), the influence of the radial terms on eigenvalue and scalar variables has been compared. Error metric on nozzle diameter effects is presented with comparison to typical experimental measurement uncertainties. The analysis also showed that, for nozzle separation distances below the free-floating limit, the self-similar function in quasi one-dimensional formulation can be preserved by specifying radial velocity boundary conditions, as long as the radial gradients are negligible.

INTRODUCTION

The theory that reduces the two-dimensional axisymmetric counterflow or opposed-jet flame configuration to a quasi one-dimensional (1D) formulation is well established and widely used throughout the combustion community (Kee et al., 1989, 2003; Seshadri and Williams, 1978; Smooke et al., 1991). The key assumptions in the derivation of quasi 1D theory are (i) description of the radial flow velocity via a self-similarity function, $v_r = rU(z)$, and (ii) zero radial gradients of all scalar variables along the axis of symmetry. A direct consequence of approximations (i) and (ii) is that the radial pressure-gradient, $\Lambda = (1/r)(\partial p/\partial r)$, is treated as a constant eigenvalue along the axis of symmetry. The

validity of this theory has been well established by Seshadri and co-workers (Puri and Seshadri, 1986) in experiments using large diameter nozzles with screens (typically of the order of 25 mm or greater in diameter) to produce a uniform axial velocity profile at the nozzle exits (see Figure 1a), with a nozzle separation distance of about 14 mm.

The above ideal large diameter nozzle counterflow configuration cannot always be realized in experiments. For example, in conducting studies at extreme pressure or strain rate conditions, two-phase flows, or when performing advanced laser-based diagnostics, small diameter nozzles are beneficial and have been explored by many researchers (Mittal et al., 2012; Wu and Law, 1984). The inconsistencies that could arise from applying quasi 1D theory of Seshadri and Williams (1978) to small diameter nozzles has been a topic of great interest. Specifically, it is important to quantify the uncertainties introduced in applying quasi 1D theory to counterflow flames if such data is to be used in chemical kinetic model optimization or validation investigations.

As first shown by Rolon et al. (1991), experiments with converging nozzles with large area ratios (without screens) suffer from nonuniform axial velocities as the nozzle separation distance is reduced from an ideal separation distance that yielded a plug flow profile (see Figure 1b). A consequence of such nonideal flow separation distance is that the assumed zero axial velocity gradient in the axial direction at the nozzle exit, $\partial v_z / \partial z = 0$ (or $U(z) = 0$ via continuity equation $\partial (\rho v_z) / \partial z = -2\rho U(z)$ with constant density in the cold invicid flow region), is not satisfied in such experiments. A method for correcting this inconsistent finite $U(z)$ in quasi 1D simulations with nonideal nozzle separation distances was first proposed by Chelliah et al. (1991). Subsequent work by Dimotakis and co-workers (Bergthorson et al., 2005, 2011) and by Sarnacki et al. (2012) further highlighted the importance of proper boundary conditions with nozzle separation distance. In particular, for premixed flames stabilized over a stagnation plate with heat losses, Bergthorson et al. (2005, 2011) have shown that the reacting viscous boundary layer is invariant with the nozzle separation distance once the nozzle separation distance is in the free-jet regime. It is important to note that the quasi 1D theory cannot be applied to freejet regime irrespective of the nozzle diameter. In contrast to stagnation flame-plate configuration, counterflow or opposed-jet laminar flames cannot be stabilized at large nozzle separation distances without some anchoring mechanism (see Figure 1b). The nozzle separation distance at which they are barely anchored is identified as the freely-floating regime, $L = L_{FF}$ (Pellett et al., 1991; Sarnacki et al., 2012). Moreover, Sarnacki et al. (2012) experimentally demonstrated that, as this ideal nozzle separation distance that yields a plug-flow profile is approached, the flame extinction strain rate defined by the Seshadri and Williams theory (identified here as a_{theory}) agrees with the local extinction strain rate (identified as a_{local}), within the experimental uncertainties.

The first 2D numerical investigation on small diameter nozzles in counterflow flames was performed by Frouzakis et al., (1998) using the axisymmetric configuration. The main focus of their investigation was the effect of nozzle exit velocity profiles (i.e., plug versus parabolic flow) on predicted non-premixed flame structure, for a specific nozzle diameter ($D = 10$ mm) and separation distance ($L = 10$ mm). In their axisymmetric simulations, the pressure eigenvalue, Λ, was shown to deviate from the constant value in quasi 1D formulation, especially in the cold region where local flow strain rate is quantified. It was reported that this deviation reduced as the diameter of the nozzle was doubled, without providing any quantitative information. The study's main conclusion was that quasi 1D formulation is adequate as long as a uniform velocity or plug flow condition is satisfied at the nozzle exit, without any explicit recommendation or guidance on preferred L or D to be used in experiments. In a more recent axisymmetric numerical investigation on twin-premixed
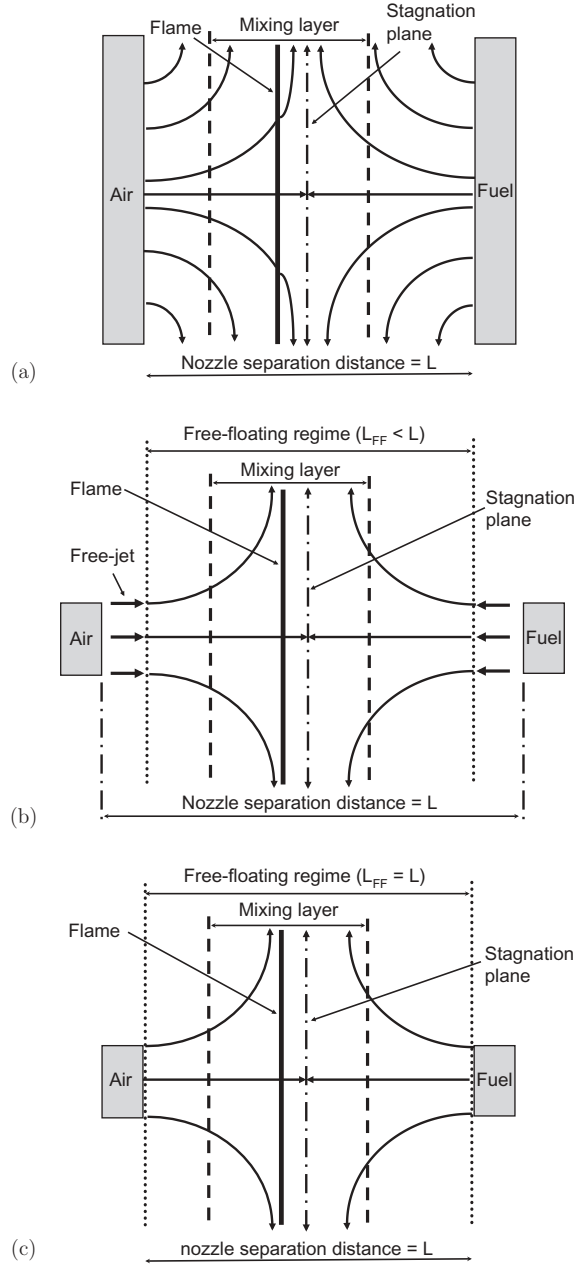
Figure 1 Schematic of counterflow diameter and separation distance effects: (a) large nozzle setup (Seshadri type burner) with plug-flow velocity profile, (b) small diameter nozzles with non-ideal separation distances ($L > L_{FF}$ with plug flow and free-jet or $L < L_{FF}$ with finite U values), and (c) small nozzles with ideal separation distance ($L = L_{FF}$).

counterflow flames using 14 mm nozzles, Mittal et al. (2012) have shown that the inclusion of radial heat conduction term in quasi 1D simulations has much greater effect than the eigenvalue departure from a constant value. The main goal of the investigation was to

determine the flame stretch effects on premixed burning velocity. Bouvet et al. (2013) also performed axisymmetric numerical investigations on a premixed flame-plate configuration using a 7-mm nozzle, including experimental measurement of the velocity field. By considering a nonreacting case with an equivalent $L > L_{FF}$ (i.e., a separation distance greater than the free-floating regime where quasi 1D theory does not apply), they came to the conclusion that quasi 1D theory fails to represent the stagnation flow-plate configuration. In the reacting case, with an effective nozzle separation distance less than the free-floating regime ($L < L_{FF}$) due to thermal expansion of the reacting mixing layer, the subtle differences of the axial velocity predicted using axisymmetric and quasi 1D formulations also highlighted the inadequacy of the quasi 1D theory.

None of the aforementioned studies systematically addressed the effects of nozzle diameter on the neglected radial gradients in quasi 1D formulation. As mentioned earlier, Frouzakis et al. (1998) suggested that doubling the nozzle diameter could reduce the eigenvalue nonuniformity in the cold region. Furthermore, they stated that the average value of the eigenvalue in axisymmetric simulation is close to the constant eigenvalue assumed in quasi 1D simulations; hence, the quasi 1D formulation is acceptable for the small diameter nozzle considered. In experiments, Sarnacki et al. (2012) attempted to address the nozzle diameter effect on counterflow flame extinction limits, however, the two nozzles used (7 mm and 15 mm) were not identical in area contraction ratio leading to two different boundary layers at the nozzle exits and they failed to draw any meaningful conclusions. Here, by using a consistent nozzle geometry generated by minimization of Görtler vorticity formation (see Bergthorson et al., 2005), the effects of nozzle diameter versus separation distance on the quasi 1D formulation is analyzed numerically.

In the axisymmetric numerical analysis presented here, the OpenFOAM computational package was used to integrate the governing equations with a Finite Volume Method solver, that includes the detailed transport and chemical kinetic models (Jasak et al., 2007). To lower computational cost, diluted hydrogen versus air counterflow non-premixed flame with a modest extinction strain rate of around $400 \, \text{s}^{-1}$ was considered. Such strain rates are close to the extinction limits of methane-air non-premixed flames and other mildly diluted hydrocarbon-air extinction limits; hence, these conditions are of great relevance. In addition, in both axisymmetric and quasi 1D simulations, the Soret effects were neglected. Several computational geometries corresponding to Seshadri type and small diameter nozzle type configurations (see Figure 1) were considered to highlight the differences between quasi 1D and full counterflow geometry simulations on flame structure as well as extinction limit predictions.

GOVERNING EQUATIONS AND NUMERICAL APPROACH

The reacting Navier–Stokes equations that describe the conservation of mass, momentum, energy, and species of axisymmetric counterflow field are well known (Kee et al., 2003; Williams, 1985), and for brevity, only the essential features are presented here. A key difference between the 2D axisymmetric (OpenFOAM) and the quasi 1D implementation is that the equations are written in conservative and non-conservative form, respectively (see the appendix for a complete mathematical formulation). The two conservation equations of importance for the present discussion are the steady state radial momentum and the energy conservation equations—in 2D axisymmetric implementation:

$$\rho v \frac{\partial v_r}{\partial z} + \rho v_r \frac{\partial v_r}{\partial_r} = -\frac{\partial p}{\partial r} + \frac{\partial}{\partial z}\left(\mu \frac{\partial v_r}{\partial z}\right) + \underbrace{\left\{\frac{\partial}{\partial r}\left(\frac{\mu}{r}\frac{\partial v_r}{\partial r}\right)\right\}}_{\text{Term1}} \tag{1}$$

$$\frac{\partial}{\partial z}(\rho v h_s) - \frac{\partial}{\partial z}\left(\rho\alpha\frac{\partial h_s}{\partial z}\right) + \frac{\partial}{\partial z}\left(\sum_{i=1}^{N}\rho h_i^s \overrightarrow{V}_{z,i}\right)$$

$$= -\sum_{i=1}^{N} h_i^0 w_i + \underbrace{\left\{-\frac{\partial}{\partial r}(\rho v_r h_s) + \frac{\partial}{\partial r}\left(\rho\alpha\frac{\partial h_s}{\partial r}\right) - \frac{\partial}{\partial r}\left(\sum_{i=1}^{N}\rho h_i^s \overrightarrow{V}_{r,i}\right)\right\}}_{\text{Term 2}} \tag{2}$$

and in quasi 1D theory implementation with $v_r = rU(z)$:

$$\rho v \frac{\partial U}{\partial z} + \rho U^2 = -\frac{1}{r}\frac{\partial p}{\partial r} + \frac{\partial}{\partial z}\left(\mu \frac{\partial U}{\partial z}\right) \tag{3}$$

$$\rho v \frac{\partial h_s}{\partial z} - \frac{\partial}{\partial z}\left(\alpha \frac{\partial h_s}{\partial z}\right) + \frac{\partial}{\partial z}\left(\sum_{i=1}^{N}\rho h_i^s V_{z,i}\right) = -\sum_{i=1}^{N} h_i^0 w_i \tag{4}$$

In Eqs. (1) and (2), the Term1 and Term2 are the contributions due to radial effects, for example if the flame should experience any radial gradients due to small nozzle diameters.

In the OpenFOAM solver, the 2D axisymmetric conservation equations [Eqs. (A.1)–(A.4)] were integrated using the Finite Volume Method in a segregated manner. The finite volume terms were calculated using second-order accurate total variation diminishing (TVD) Van–Leer schemes (Hirsch, 2007). For low-speed reacting flows, an iterative process was implemented to solve for the pressure field as there is no efficient explicit equation for pressure at low Mach numbers. This solver used the pressure implicit splitting of operators (PISO) method (Issa, 1986), which iterates between the solved velocity field and a guessed pressure field until a specified numerical tolerance is met. For the hydrogen-air system considered, the chemical source terms were described using a detailed chemical kinetic model consisting of 11 species in 29 reactions, which was extracted from the JetSurf2.0 model (Wang et al., 2011). All transport and thermodynamic quantities were calculated using the same approach as the Sandia Transport Package (Kee et al., 1986) and thermodynamic database (Kee et al., 1993), respectively, and were integrated into the OpemFOAM solver. To verify the implementation of the OpenFOAM solver, several canonical reacting flow configurations were considered and are described in the appendix.

In the quasi 1D implementation, the conservation equations were integrated using Smooke's counterflow code (Smooke et al., 1991) as well as the Sandia Oppdif code (Lutz et al., 1997). The same chemical kinetic model parameters as well as the transport coefficients were implemented for comparisons with the 2D axisymmetric (OpenFOAM) solution.

Computational Domain

For a Seshadri type burner having large diameter nozzles ($D = 26$ mm), an axisymmetric computational domain having a wedge-shaped mesh (see Figure 2a) with uniform velocity profiles at fuel and air exit planes was considered (i.e., without nitrogen co-flow), as shown in Figure 2b. For smaller diameter nozzles, a computational domain with similar wedge-shaped mesh but with full details of the converging nozzles with annular inert nitrogen co-flow was considered, as shown in Figure 2c. As mentioned earlier, the fuel and air nozzle shapes considered were similar to those used in experiments by Sarnacki et al. (2012), which were designed to minimize vorticity generation in the convergent section. In order to analyze the small diameter effects, two grids were generated with inner nozzle
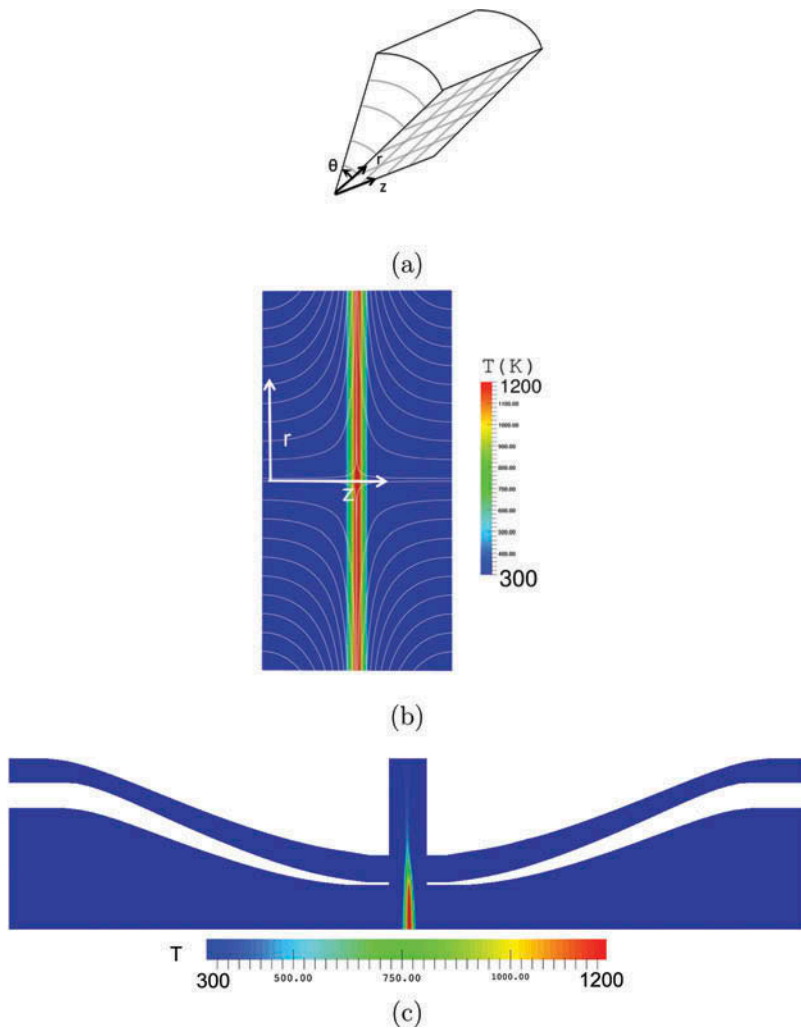
Figure 2 Computational domains implemented showing (a) 2D wedge-shape mesh with r and z coordinates, (b) typical solution from large diameter Seshadri type plug-flow burners, and (c) solution from a small diameter nozzle type burners.

diameters of 6.5 and 13 mm. Together with the Seshadri type configuration described above, the nozzle diameter effects were analyzed for $D = 6.5$, 13, and 26 mm. To address the nozzle separation distance effects, several computational grids were generated for $D = 6.5$ mm nozzles ($L = 4$ and 8 mm) and for $D = 13$ mm nozzles ($L = 5$, 9, 13, 16, and 19.5 mm).

Various structured grid refinement strategies were explored depending on the complexity of the computational domain. For example, for the Seshadri type burner computational domain (Figure 2b), a uniform grid spacing of 15 μm was used for all the cases with excellent agreement with the quasi 1D solutions. For more complex small nozzle diameter computational domains, both uniform and stretched grids were considered. In the unstretched regions, a uniform grid spacing of 30 μm was maintained with a maximum aspect ratio of 2.0. To establish grid independence, in the reacting layer the grid was refined for several cases to achieve a 15-μm grid spacing and the steady-state solutions confirmed that the results were in the asymptotic range with only 3 K change in temperature between 30 and 15 μm solutions.

Boundary Conditions

Figure 2b shows the computational domain simulated for the Seshadri type burner, while Figure 2c shows the domain for a small diameter nozzle that included the entirety of the fuel, air, and co-flow nozzles, mixing region, and outflow region. In the 2D axisymmetric simulations, the inflow planes were different depending on the computational geometry considered. The boundary conditions imposed at the inflow planes consisted of fixed velocity plug flow, Neumann condition for pressure, fixed ambient temperature ($T_0 = 300$ K), and fixed species mole fractions (diluted hydrogen ($X_{H_2} = 0.16$) versus air ($X_{O_2} = 0.21$)). The inclusion of the full nozzle geometry in the small diameter simulations allowed the plug flow upstream velocity to develop into the expected nonuniform velocity profiles at the nozzle exits. The plug-flow velocities prescribed were varied to explore strain effects on the flame. However, the precise local strain rate specification was difficult due to variation in nozzle exit velocity profile depending on the nozzle separation distance and thermal expansion. In the small diameter nozzle case, the inert nitrogen co-flow momentum was always matched with the momentum of the inner jet. This assured that the shear layer formed between the inner and the outer streams did not influence the flow divergence. Outflow boundary conditions of the computational domain were similar for all cases and were prescribed by fixing far-field pressure nodes and Neumann conditions for all other variables. Nozzle walls and edges were described by no-slip, viscous boundary conditions by setting normal and tangential velocity components to zero, and all other variables were described by Neumann conditions at the wall face. Chemical reactions were initiated by imposing a Gaussian temperature profile over a nonreacting diffusion solution and residuals were monitored to assure convergence for all solutions.

In the quasi 1D flame solutions, the pressure was held constant at the average value determined from axisymmetric simulations and the temperature and species boundary conditions imposed were the same as those described above in the 2D axisymmetric simulations. In addition, the velocity boundary conditions (v_z and U) in the quasi 1D formulation were matched with the OpenFOAM solutions (identified as OF) as described below, for large diameter nozzle (Seshadri type burner):

$$z = \pm \frac{L}{2}, \; v_z = (v_z)_{OF}, \; U = 0 \qquad (5)$$

and for small diameter nozzles:

$$L = L_{FF} : z = \pm \frac{L}{2}, \ v_z = (v_z)_{OF}, \ \ U = 0 \tag{6}$$

$$L < L_{FF} : z = \pm \frac{L}{2}, \ v_z = (v_z)_{OF}, \ \ U = U_{OF} \neq 0 \tag{7}$$

$$L > L_{FF} : quasi \ one\text{-}dimensional \ theory \ cannot \ be \ applied \tag{8}$$

RESULTS

Large Diameter Seshadri Type Burner Simulations

Based on the non-premixed flames established between opposed large diameter nozzles ($D = 26$ mm) with plug-flow velocity profiles, the key terms that support the validity of the quasi 1D theory of Seshadri and Williams (1978) are presented first. Figures 3 and 4 show a comparison of the velocity field (i.e., axial velocity, $v \equiv v_z$, and self-similarity function, $U \equiv v_r / r$) and the temperature as a function of the distance along the axis of symmetry predicted using 2D axisymmetric simulations (solid lines) and quasi 1D simulations (dashed lines). For the diluted hydrogen and air flame with a moderately high local strain rate of $a = 375$ s^{-1} (*Note*: the local extinction strain rate is about 480 s^{-1}), the velocity and temperature agreements are well within the numerical uncertainties (see section "Grid Resolution Effects" in the appendix). Certainly, the differences shown between two implementations are much smaller than the current experimental measurement techniques of flow strain rates and temperature (Figura and Gomez, 2012; Sarnacki et al., 2012).
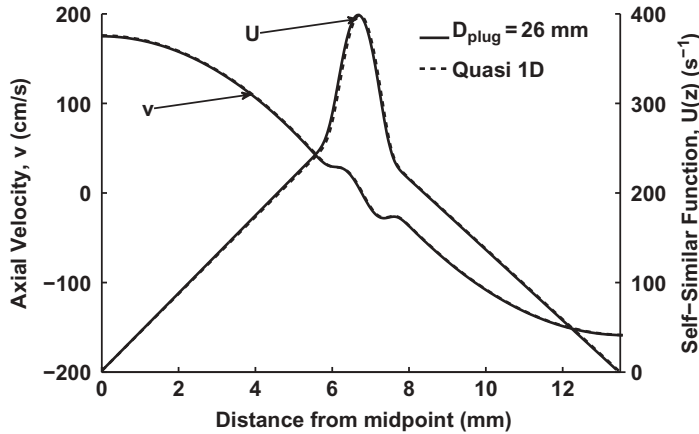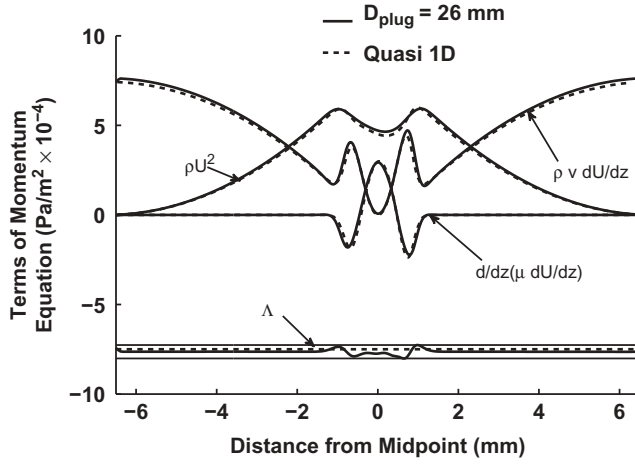

Figure 3 Comparison of axial velocity and self-similarity function ($U (z)$) using axisymmetric (OpenFOAM—solid line) and quasi one-dimensional (dashed line) simulations, for a plug flow case with a diameter of 26 mm (Seshadri type burner) and local strain rate of $a = 375$ s^{-1}.
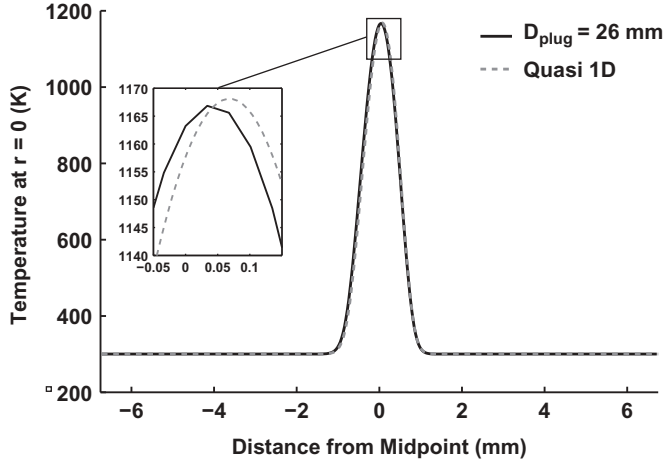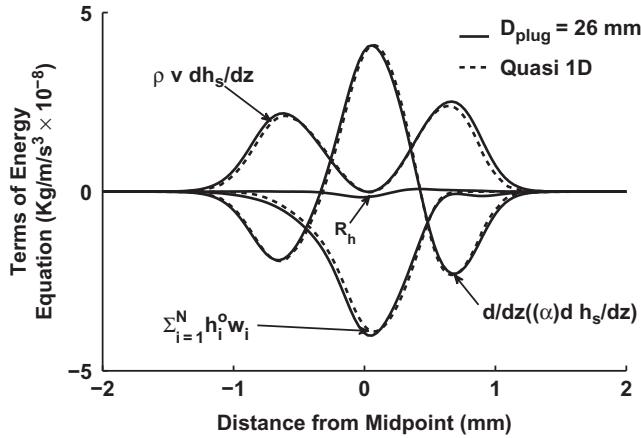
Figure 4 Comparison of flame temperature using axisymmetric (OpenFOAM—solid line) and quasi one-dimensional (dashed line) simulations, for a plug flow case with a diameter of 26 mm (Seshadri type burner) and strain rate of $a = 375$ s^{-1}.

A key observation from the above results are that (a) the self-similarity function, $U(z)$, agrees well in both cold hydrodynamic region as well as inside the reacting mixing layer region and (b) the excellent agreement implies that the radial terms included in the axisymmetric simulation are negligible. One can further evaluate the contribution of the radial terms in 2D axisymmetric formulation in comparison to the dominant axial terms. For example, in the radial momentum equation, at steady state, the only term that is neglected in the quasi 1D formulation is the Term1 identified in Eq. (1). Any finite contribution of the Term1 can be thought of as the residue in Eq. (3) and will manifest as a variation of Λ in axisymmetric simulations. This residue is identified here as R_Λ. Figure 5 shows a comparison of the eigenvalue, Λ, calculated from quasi 1D and 2D axisymmetric simulations, together with all other remaining terms contributing to the radial momentum equation, Eq. (1). For the present large diameter nozzle simulations, the departure of the eigenvalue from a constant value determined from the quasi 1D is very small $\left(\Lambda = -(7.6 \pm 0.2) \times 10^{-4} \text{ Pa}/\text{m}^2 \right)$, especially in the cold hydrodynamic region where the flow strain rate is typically calculated. In contrast, previous work with *small* diameter nozzles have reported comparatively larger departure of the eigenvalue from quasi 1D theory (Bouvet et al., 2013; Frouzakis et al., 1998; Mittal et al., 2012).

Any radial variations in counterflow flames can also influence the solution of energy and species conservation equations, i.e., scalar properties T and Y_i. In Eq. (2), Term2 identifies the radial gradient dependencies in energy conservation equation that give rise to differences between the axisymmetric and the quasi 1D solutions. For the present discussion, this residual term is identified as R_h. Figure 6 shows a comparison of all the terms in Eq. (2) evaluated using 2D axisymmetric and quasi 1D solutions, including the residue term R_h. A very small value of R_h implies that for the present large diameter Seshadri type burner with plug-flow velocity profiles, the radial term in energy equation is negligible and the quasi one-dimensional theory accurately represents the 2D axisymmetric flow field.
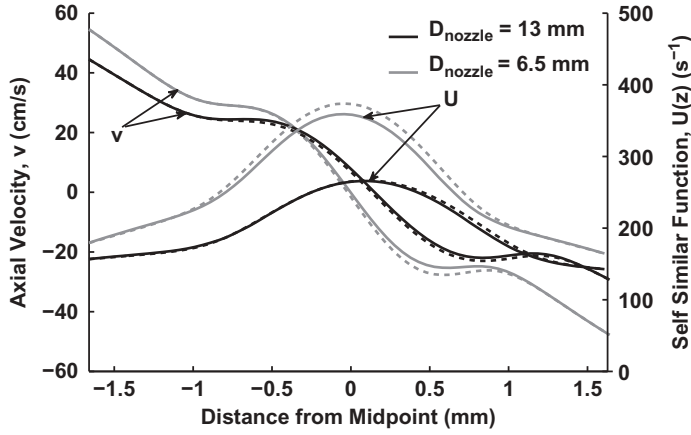
Figure 5 Comparison of the terms in radial momentum equation (including eigenvalue, Λ) using axisymmetric (OpenFOAM—solid line) and quasi one-dimensional (dashed line) simulations, for a plug flow with a diameter of 26 mm (Seshadri type burner) and strain rate of $a = 375 \text{ s}^{-1}$.
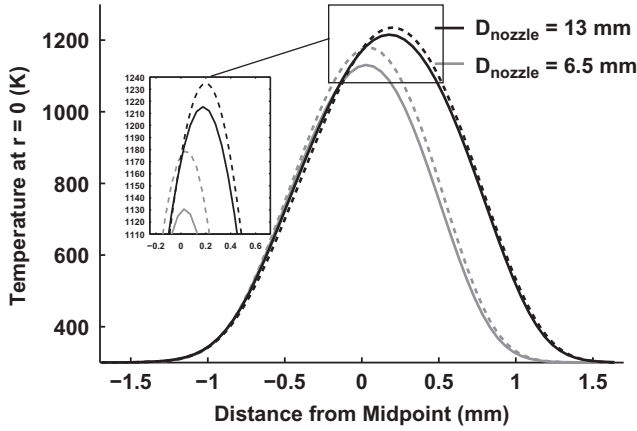

Figure 6 Comparison of the terms in the quasi one-dimensional energy equation using axisymmetric (OpenFOAM—solid line) and quasi one-dimensional (dashed line) simulations, for a plug flow with a diameter of 26 mm (Seshadri type burner) and strain rate of $a = 375 \text{ s}^{-1}$. The residue of axisymmetric solution is identified as R_h, which is mainly due to the radial heat conduction term.

Nozzle Diameter Effects

While the concept of minimizing radial effects by increasing the nozzle diameter is not new, the main purpose of the present article is to develop an error metric to quantify the effect of radial contributions in small diameter counterflow flames, as a function of both the nozzle diameter and the nozzle separation distance. To our knowledge, such a systematic investigation has not been reported in the literature, which is now possible due to advanced computational capabilities available. For two nozzle diameters of $D = 13$ and 6.5 mm with a nozzle separation distance of $L = 4$ mm, Figures 7–10 show comparisons of the velocity
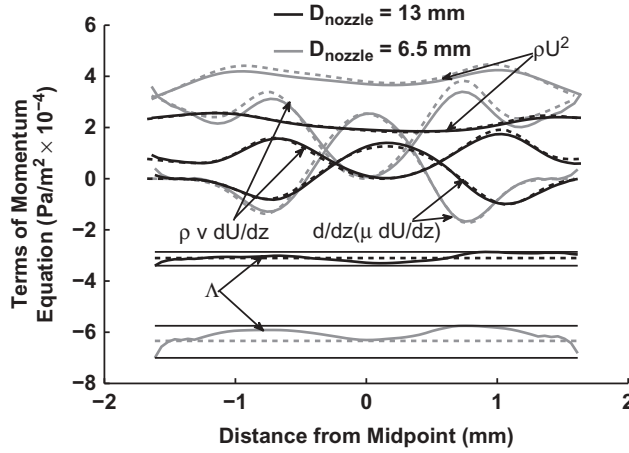
Figure 7 Comparison of axial velocity and self-similarity function ($U(z)$) using axisymmetric (OpenFOAM—solid line) and quasi one-dimensional (dashed line) simulations, for (i) nozzle flow with diameter of 13 mm and strain rate of $a = 268$ s^{-1}, and (ii) nozzle flow with diameter of 6.5 mm and strain rate of $a = 354$ s^{-1}.
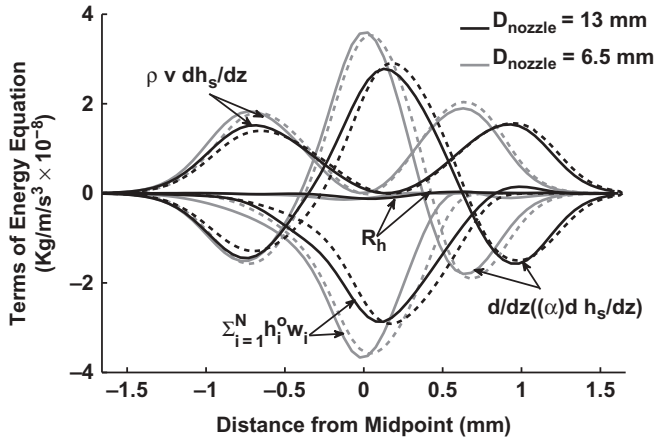

Figure 8 Comparison of flame temperature using axisymmetric (OpenFOAM—solid line) and quasi one-dimensional (dashed line) simulations, for (i) nozzle flow with diameter of 13 mm and strain rate of $a = 268$ s^{-1} and (ii) nozzle flow with diameter of 6.5 mm and strain rate of $a = 354$ s^{-1}.

field and temperature, terms contributing to the radial momentum equation and energy conservation equation, respectively, predicted using the 2D axisymmetric simulations and quasi 1D simulations. Since $L < L_{FF}$ with finite U values at the nozzle exit planes, in quasi 1D simulations, both $v_{z,\pm L/2}$ and $U_{\pm L/2}$ values from 2D simulations are imposed. Alternatively, if these boundary conditions are available from experiments, for example, from PIV measurements (Sarnacki et al., 2012), they can be imposed in quasi 1D simulations. While the local strain rates are different for the two nozzle diameters considered ($a = 268$ s^{-1} for $D = 13$ mm and $a = 354$ s^{-1} for $D = 6.5$ mm), a small but noticeable difference of the flame structure between the 2D axisymmetric and quasi 1D simulations is observed. In particular, the residual term R_h in energy equation (see Figure 11) shows an increased departure as the nozzle diameter is reduced from 13 mm to 6.5 mm. A quantitative comparison of

Figure 9 Comparison of the terms in radial momentum equation (including eigenvalue, Λ) using axisymmetric (OpenFOAM—solid line) and quasi one-dimensional (dashed line) simulations, for (i) nozzle flow with diameter of 13 mm and strain rate of $a = 268$ s^{-1} and (ii) nozzle flow with diameter of 6.5 mm and strain rate of $a = 354$ s^{-1}.

Figure 10 Comparison of the terms in the quasi one-dimensional energy equation using axisymmetric (OpenFOAM—solid line) and quasi one-dimensional (dashed line) simulations, for (i) nozzle flow with diameter of 13 mm and strain rate of $a = 268$ s^{-1} and (ii) nozzle flow with diameter of 13 mm and strain rate of $a = 354$ s^{-1}. The residue of axisymmetric solution is identified as R_h, which is mainly due to the radial heat conduction term.

diameter effects on Λ, R_h, and U is presented in the section, "Metric for Quantification of Radial Effects."

For the smaller diameter nozzles ($D = 6.5$ mm), the temperature comparisons shown in Figure 8 indicate 46 K difference in peak flame temperature between the 2D axisymmetric and quasi 1D simulations. This difference is certainly greater than any numerical effects discussed in the appendix (of the order of 10 K). In contrast, for the larger diameter nozzle ($D = 13$ mm), difference in predicted peak temperature is 20 K. Since accurate
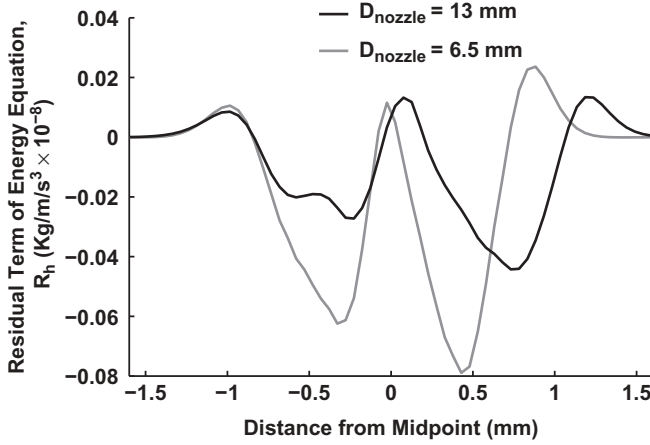
Figure 11 Comparison of the residue term only in the energy equation (R_h), for (i) nozzle flow with diameter of 13 mm and strain rate of $a = 268 \text{ s}^{-1}$ and (ii) nozzle flow with diameter of 13 mm and strain rate of $a = 354 \text{ s}^{-1}$.

estimation of flame temperature is critical for chemical kinetic model validation, it is important to understand the origin of these temperature variations. The first clue is that, for the $D = 6.5$ mm nozzle, the deviation of self-similar function U between the two simulations is significant irrespective of the specification of the exact axial velocity and U values at the boundaries (see Figure 7). Examination of the terms contributing to the radial momentum equation (Figure 9) shows that while most terms are of the same order, the eigenvalue spread is significantly large for the $D = 6.5$ mm case in comparison to the $D = 13$ mm nozzles. Secondly, consistent with the analysis by Mittal et al. (2012), the residue of the energy equation is dominated by the radial heat conduction term and increases with decreasing the nozzle diameter (see Figure 11).

Nozzle Separation Distance Effects

Unlike in the Seshadri type burner with screens, in *small* diameter nozzle experiments it is impossible to determine a priori the *ideal* nozzle separation distance where $U = 0$ at the boundaries. This is because of the variability of the mixing layer thickness, L_{mixing}, which depends on the thermal expansion associated with the overall heat release and the imposed flow strain rates (or the Reynolds number). Thus, in quasi 1D simulation of small diameter counterflow experiments with an arbitrarily selected nozzle separation distance, the finite U values at the boundaries must be either measured from experiments, or calculated as in present 2D simulations. The fundamental assumption in such quasi 1D calculations with imposed finite U values is that the radial gradients are negligible irrespective of the nozzle diameter. To explore the applicability of this assumption, 2D axisymmetric calculations were carried out for several different nozzle separation distances using both nozzle diameters considered above. For brevity, only the smaller diameter nozzles' results are presented here. Figures 12–15 show a comparison between the 2D axisymmetric results and the quasi 1D simulations for $L = 4$ and 8 mm. Qualitatively, smaller separation distance simulations with imposed finite U values seem to yield results in closer agreement with the 2D axisymmetric simulations.
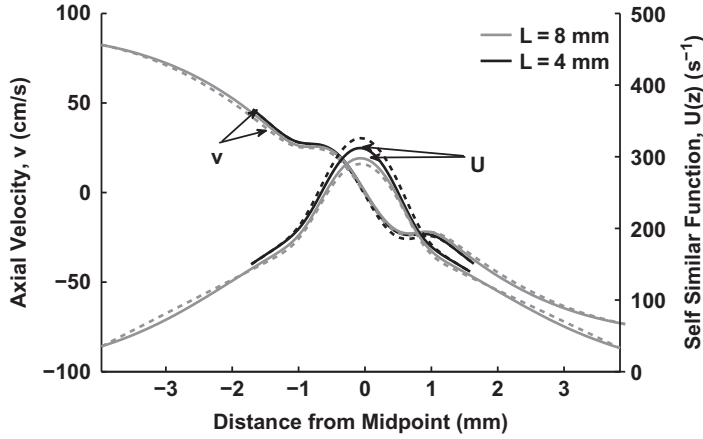
Figure 12 Comparison of axial velocity and self-similarity function ($U(z)$) using axisymmetric (OpenFOAM—solid line) and quasi one-dimensional (dashed line) simulations, for two separation distances using 6.5 mm nozzles (i) $L = 8$ mm and strain rate of $a = 290$ s^{-1} and (ii) $L = 4$ mm and strain rate of $a = 354$ s^{-1}.
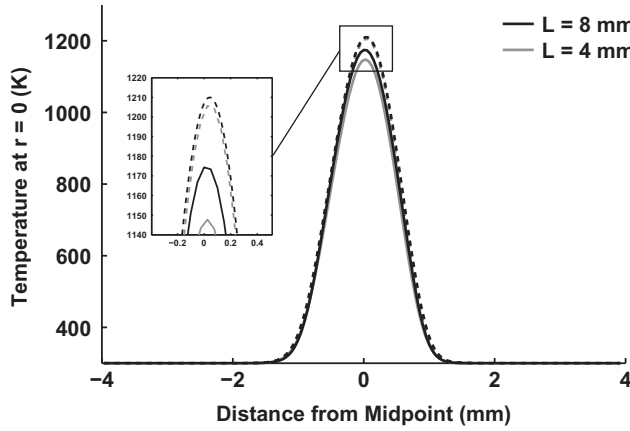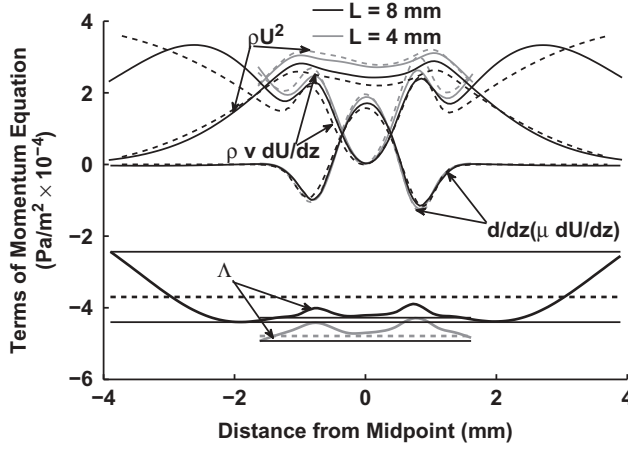

Figure 13 Comparison of temperature using axisymmetric (OpenFOAM—solid line) and quasi one-dimensional (dashed line) simulations, for two separation distances using 6.5 mm nozzles (i) $L = 8$ mm and strain rate of $a = 290$ s^{-1} and (ii) $L = 4$ mm and strain rate of $a = 354$ s^{-1}.

## Metric for Quantification of Radial Effects

Instead of making qualitative comparisons between 2D axisymmetric and quasi 1D simulations, a quantitative estimate of the neglected radial terms can be evaluated by suitably defined error metric, for example the L_2-norm given by:

$$L_2\left(\phi_i\right) = \sqrt{\frac{\sum_{j=1}^{N_c} \left(\phi_i\right)_j^2}{N_c}} \tag{9}$$

where $\phi_i^2 = (\Lambda_{2D} - \Lambda_{1D})^2$, R_h^2, or $(U_{2D} - U_{1D})^2$ are summed over computational cells, N_c, from $j = 1, \ldots, N_c$ along the axis of symmetry. Figures 16 and 17 show comparisons

Figure 14 Comparison of the terms in radial momentum equation (including eigenvalue, Λ) using axisymmetric (OpenFOAM—solid line) and quasi one-dimensional (dashed line) simulations, for two separation distances using 6.5 mm nozzles (i) $L = 8$ mm and strain rate of $a = 290$ s^{-1} and (ii) $L = 4$ mm and strain rate of $a = 354$ s^{-1}.
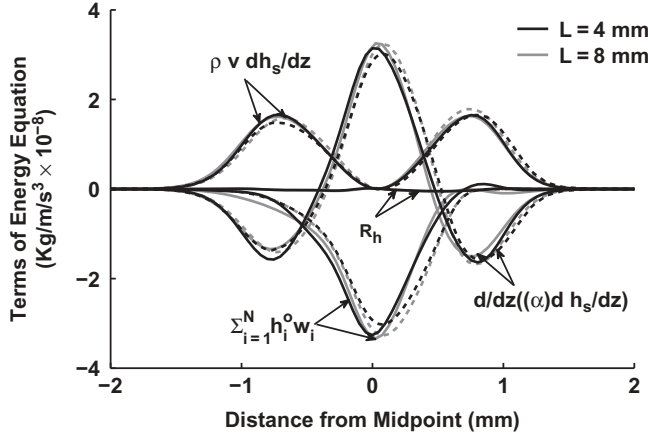

Figure 15 Comparison of the terms in quasi one-dimensional energy equation using axisymmetric (OpenFOAM—solid line) and quasi one-dimensional (dashed line) simulations, for two separation distances using 6.5 mm nozzles (i) $L = 8$ mm and strain rate of $a = 290$ s^{-1} and (ii) $L = 4$ mm and strain rate of $a = 354$ s^{-1}. The residue of axisymmetric solution is identified as R_h, which is mainly due to the radial heat conduction term.
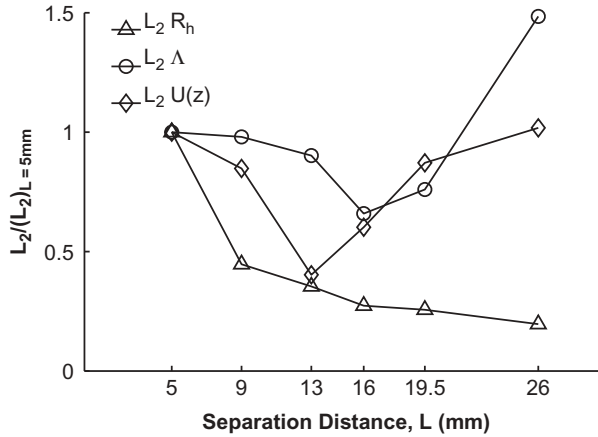
of such a metric as a function of the nozzle diameter and nozzle separation distance, respectively.

The large diameter Seshadri type burners clearly yield the lowest L_2-norm as seen from Figure 16. However, it may be useful to correlate the error metric to typical measurement uncertainties and explore the existence of an optimal nozzle diameter and separation distance or a range in applying quasi 1D theory. To address this question, the eigenvalue variance shown in Figure 9 is first correlated with the local strain rate variations. For example, in the case of diluted hydrogen and air flame considered, for $D = 13$ mm case, the predicted eigenvalue variation between -2.86×10^{-4} to -3.4×10^{-4} Pa/m^2 corresponds to a local strain rate variation of 267 s^{-1} to 275 s^{-1} and to a peak flame
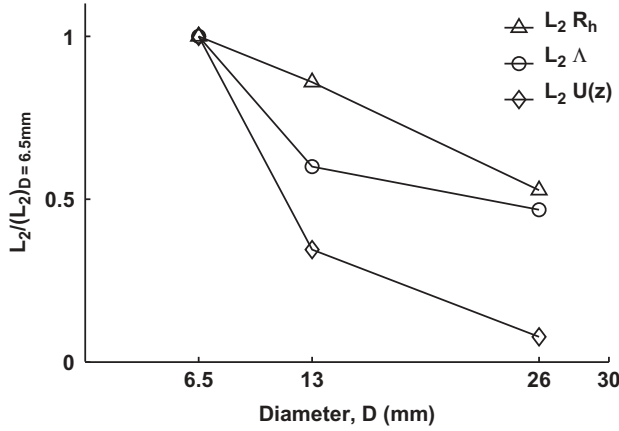
Figure 16 Comparison of the L_2-norm evaluated based on Λ, R_h, and U as a function of the nozzle diameter, for nozzle separation distance of $L = 4$ mm. *Note*: L_2-norm values are normalized by those at $D = 6.5$ mm.

Figure 17 Comparison of the L_2-norm evaluated based on Λ, R_h, and U as a function of the nozzle separation distance, for nozzle diameter of $D = 13$ mm. *Note*: L_2-norm values are normalized by those at $L = 5$ mm.

temperature variation of 1228 K to 1240 K. These variations are well within the current measurement uncertainties (Figura and Gomez, 2012; Sarnacki et al., 2012). Even for the smaller diameter nozzle considered, the eigenvalue variation between -5.75×10^{-4} to -7.0×10^{-4} Pa/m^2 yields very modest local strain rate variations between 328 s^{-1} to 339 s^{-1} and peak flame temperature variations of 1167 K to 1185 K, again well within the experimental measurement uncertainties, but greater than the numerical uncertainties.

Figure 17 shows the variation of error metrics for the large diameter nozzle as a function of nozzle separation distance. For $L < L_{FF}$, with the inclusion of finite radial velocity gradient effects [i.e., finite U—see Eq. (7)] in the quasi 1D calculations, increase in L yields a lower error. This reduction in error can be related to lower radial gradients as the nozzles are pulled apart. However, as the nozzle separation distance approaches or exceeds the free-floating limit (i.e., $L > L_{FF}$), where quasi 1D theory is not applicable [see Eq. (8)], the error metric is seen to increase.

While this investigation considered only a limited range of flame strain rate variations (slightly away from flame extinction limit), based on the above discussion, it may be reasonable to conclude that as long as finite U values are imposed at the boundaries, small diameter nozzle experiments with nozzle diameters of the order of 12 mm or greater can be used with quasi 1D simulations. Furthermore, for 13-mm diameter nozzles $1 < L/D < L_{FF}/D$ is seen to yield the lowest departure between 2D and quasi 1D solutions. Whether this finding can be generalized to any small diameter nozzles is not clear. One essential requirement in applying the quasi 1D theory is that the nozzle separation distance must lie between the free-floating distance and the mixing layer thickness. Violation of the latter will lead to heat losses at the nozzles.

CONCLUSIONS

2D axisymmetric counterflow reacting flow simulations were performed to investigate the applicability of quasi 1D theory of Seshadri and Williams to small diameter, large area-ratio converging nozzles. Analysis was also performed with large diameter nozzles with plug flow boundary conditions (Seshadri type burners) to demonstrate the negligible effects of the radial terms in conservation equations. When applied to smaller diameter converging nozzles, the influence of non-zero contributions of radial terms on radial momentum and energy conservation equations were explicitly evaluated. Based on a normalized error metric, and the diluted hydrogen versus air non-premixed flames considered, it was suggested that nozzle diameters greater than 12 mm will yield errors less than numerical uncertainties and certainly well below current experimental uncertainties. With regard to nozzle separation distance, analysis was performed for distances greater than the mixing layer distance and lower than the free-floating regime distance. It was shown that, as long as radial effects are small, specification of finite values for the self-similar function at the boundaries in quasi 1D simulations can predict the flow strain rates and flame temperature within numerical or experimental uncertainties.

While the verification of the 2D OpenFOAM numerical solver was performed by considering chemical source term integrations, premixed flame structure solutions, and non-premixed flame extinction limit predictions using simpler Seshadri type burner configuration, further work is needed to establish the nozzle-based extinction limit predictions. Once completed, the solver developed with parallel computing capabilities can provide a valuable tool for future multi-dimensional laminar flame investigations with detailed chemical kinetic models.

ACKNOWLEDGMENT

FUNDING

REFERENCES

Bergthorson, J.M., Salusbury, S.D., and Dimotakis, P.E. 2011. Experiments and modelling of premixed laminar stagnation flame hydrodynamics. *J. Fluid Mech.*, **681**, 340–369.

Bergthorson, J.M., Sone, K., Mattner, T.W., Dimotakis, P.E., Goodwin, D.G., and Meiron, D.I. 2005. Impinging laminar jets at moderate reynolds numbers and separation distances. *Phys. Rev. E*, **72**, 066307-1–066307-12.

Bouvet, N., Davidenko, D., Chauveau, C., Pillier, L., and Yoon, Y. 2013. On the simulation of laminar strained flames in stagnation flows: 1D and 2D approaches versus experiments. *Combust. Flame*, **161**(2), 438–452

Chelliah, H.K., Law, C.K., Ueda, T., Smooke, M.D., and Williams, F.A. 1991. An experimental and theoretical investigation of flow-field, dilution and pressure effects on the extinction condition of methane/oxygen/nitrogen diffusion flames. *Proc. Combust. Inst.*, **23**, 503–511.

Cuoci, A., Frassoldati, A., Faravelli, T., and Ranzi, E. 2013. A computational tool for the detailed kinetic modeling of laminar flames: Application to C_2H_4 / CH_4 coflow flames. *Combust. Flame*, **160**, 870–886.

Figura, L., and Gomez, A. 2012. Laminar counterflow steady diffusion flames under high pressure conditions. *Combust. Flame*, **159**(1), 142–150.

Frouzakis, C.E., Lee, J., Tomboulides, A.G., and Boulouchos, K. 1998. Two-dimensional direct numerical simulation of opposed-jet hydrogen-air diffusion flame. *Proc. Combust. Inst.*, **27**, 571–577.

Hirsch, C. 2007. *Numerical Computation of Internal and External Flows*, second ed., Butterworth-Heinemann, Oxford.

Issa, R.I. 1986. The computation of compressible and incompressible recirculating flows by a non-iterative implicit scheme. *J. Comput. Phys.*, **62**, 66–82.

Jasak, H., Jemcov, A., and Tukovic, Z. 2007. Openfoam: A c++ library for complex physics simulations. Presented at the International Workshop on Coupled Methods in Numerical Dynamics, IUC, Dubrovnik, Croatia, September 19–21.

Kee, R.J., Coltrin, M.E., and Glarborg, P. 2003. *Chemically Reacting Flow*, John Wiley and Sons, Hoboken, NJ.

Kee, R.J., Grcar, J.F., Smooke, M.D., Miller, J.A., and Meeks, E. 1998. Premix: A fortran program for modeling steady laminar one-dimensional premixed flames. Technical Report SAND 1998, Sandia Report.

Kee, R.J., Miller, J.A., Evans, G.H., and Dixon-Lewis, G. 1989. A computational model of the structure and extinction of strained, opposed flow, premixed methane-air flames. *Proc. Combust. Inst.* **22**(1), 1479–1494.

Kee, R.J., Miller, J.A., and Warnatz, J. 1986. A fortran computer code package for the evaluation of gas-phase multicomponent transport properties. Technical Report SAND86, Sandia Report.

Kee, R.J., Rupley, F.M., and Miller, J.A. 1993. Chemkin-ii: A fortran chemical kinetics package for the analysis of gas phase chemical kinetics. Technical Report SAND89-8009B, Sandia Report.

Lutz, A.E., Kee, R.J., Grcar, J.F., and Rupley, F.M. 1997. Oppdif: A fortran program for computing opposed-flow diffusion flames. Technical Report SAND 1997, Sandia Report.

Lutz, A., Kee, R.J., and Miller, J.A. 1987. Senkin: A fortran program for predicting homogeneous gas phase chemical kinetics with sensitivity analysis. Technical Report SAND87, Sandia National Laboratories Report.

Mittal, V., Pitsch, H., and Egolfopoulos, F. 2012. Assessment of counterflow to measure laminar burning velocities using direct numerical simulations. *Combust. Theor. Modell.*, **16**(3), 419–433.

Oevermann, M., Gerber, S., and Behrendt, F. 2009. Euler-Lagrange/DEM simulation of wood gasification in a bubbling fluidized bed reactor. *Particuology* **4**, 307–316.

Pellett, G.L., Northam, G.B., and Wilson, L.G. 1991. Counterflow diffusion flames of hydrogen, and hydrogen plus methane, ethylene, propane, and silane vs. air. AIAA 1991–0370. AIAA Aerospace Sciences Meeting, Washington, DC, January 7–10.

Puri, I.K., and Seshadri, K. 1986. Extinction of diffusion flames burning diluted methane and diluted propane in diluted air. *Combust. Flame*, **65**, 137–150.

Reinelt, D., Laurs, A., and Adomeit, G. 1998. Ignition and combustion of a packed bed in a stagnation point flow Part II: Heterogeneous and homogeneous reactions. *Combust. Flame*, **113**(3), 373–379.

Rolon, J.C., Veynante, D., Martin, J.P., and Durst, E. 1991. Counter jet stagnation flows. *Exp. Fluids*, **11**, 313–324.

Roy, C.J., and Oberkampf, W.L. 2010. *Verification and Validation in Scientific Computing*. Cambridge University Press, Cambridge, UK.

Sarnacki, B.G., Esposito, G., Krauss, R.H., and Chelliah, H.K. 2012. Extinction limits and associated uncertainties of nonpremixed counterflow flames of methane, ethylene, propylene and n-butane in air. *Combust. Flame*, **159**, 1026–1043.

Seshadri, K., and Williams, F.A. 1978. Laminar flow between parallel plates with injection of a reactant at high reynolds number. *Int. J. Heat Mass Transfer*, **21**, 251–253.

Smooke, M.D., Crump, J., Seshadri, K., and Giovangigli, V. 1991. Comparison between experimental measurements and numerical calculations of the structure of counterflow, diluted, methane-air, premixed flames. *Proc. Combust. Inst.*, **23**(1), 463–470.

Wang, H., Dames, E., Sirjean, B., Sheen, D.A., Tangko, R., Violi, A., Lai, J.Y.W., Egolfopoulos, F.N., Davidson, D.F., Hanson, R.K., Bowman, C.T., Law, C.K., Tsang, W., Cernansky, N.P., Miller, D.L., and Lindstedt, R.P. 2011. A high-temperature chemical kinetic model of n-alkane (up to n-dodecane), cyclohexane, and methyl-, ethyl-, n-propyl and n-butyl-cyclohexane oxidation at high temperatures (jetsurf 2.0). Technical report, Combustion Kinetics Laboratory, University of Southern California. Available at: http://melchior.usc.edu/JetSurF/JetSurF2.0/Index.html

Williams, F.A. 1985. *Combustion Theory*, Westview Press, Boston.

Wu, C.K., and Law, C.K. 1984. On the determination of laminar flame speeds from stretched flames. *Proc. Combust. Inst.*, **20**, 1941–1949.

APPENDIX: VERIFICATION OF OPENFOAM NUMERICAL SOLVER

The OpenFOAM computational package was used to integrate the following reacting Navier–Stokes equations:

$$\frac{\partial \rho}{\partial t} + \nabla \cdot \rho \vec{v} = 0 \tag{A.1}$$

$$\frac{\partial \rho \vec{v}}{\partial t} + \nabla \cdot (\rho \vec{v} \vec{v}) = -\nabla p + \nabla \cdot \mathbb{T} \tag{A.2}$$

$$\frac{\partial \rho h_s}{\partial t} + \nabla \cdot \rho \vec{v} h_s - \nabla \cdot \rho \alpha \nabla h_s + \nabla \cdot \sum_{i=1}^{N} \rho h_i^s \vec{V}_i = -\sum_{i=1}^{N} h_i^0 w_i \tag{A.3}$$

$$\frac{\partial \rho Y_i}{\partial t} + \nabla \cdot \rho \vec{v} Y_i - \nabla \cdot \rho D_i \nabla Y_i = w_i, \quad i = 1, \dots, N \tag{A.4}$$

where ρ is the density, $\vec{v}$ the velocity vector, p the pressure, $\mathbb{T}$ the deviatoric stress tensor, h_s the sensible enthalpy, and α the thermal diffusivity of the mixture. For species i, Y_i is the mass fraction, D_i the mixture average diffusion coefficient, $\vec{V}_i$ the mixture average diffusion velocity, h_i^0 the chemical enthalpy, h_i^s the sensible enthalpy, and w_i the mass production rate. The conservation equations were solved in a segregated manner using second-order accurate total variation diminishing (TVD) Van–Leer schemes. The finite volume equations were integrated in time using the first-order implicit, Eulerian method. Each equation is

solved by iterating until the L_2-norm of the residual to all equations were less than 10^{-9}. Simulations were run until steady state was reached. For the purpose of this work, steady state conditions were reached when the norms of all residuals were stationary.

There is no computationally efficient equation that can be used to solve for the pressure field of low Mach number reacting flows. To calculate pressure, the work presented here used the pressure implicit splitting of operators (PISO) method (Issa, 1986), which iterates between the solved velocity field and a guessed pressure distribution until a specified numerical tolerance is met. This pressure-solving technique is computationally efficient and has precedence in the combustion community (see Cuoci et al., 2013; Oevermann et al., 2009; Reinelt et al., 1998).

The sections that follow cover in detail the verification of the OpenFOAM solver via comparison of the 2D solutions with a set of canonical combustion cases simulations.

### Chemistry Source Term Integration

A direct comparison study was performed in order to verify the correct time integration of chemical source terms by the OpenFOAM solver. The ignition of a homogeneous mixture at constant pressure and enthalpy was simulated with initial mole fraction of $X_{H_2} = 0.17$, $X_{O_2} = 0.17$, and $X_{N_2} = 0.66$. This homogeneous combustion case was verified against Sandia SENKIN solver (Lutz et al., 1987) and the results are shown in Figure 18. This was repeated for several different homogeneous mixture concentrations with the results showing the same consistency.

Premixed One-Dimensional Reacting Flow Solution

A direct comparison study was also performed between the OpenFOAM solver and Sandia 1D premixed flame code (Kee et al., 1998) by considering the spatially varying chemical reactor with a specified constant temperature. The inflow conditions considered were velocity of 2 m/s, species mole fractions of $X_{H_2} = 0.004$, $X_{O_2} = 0.001$, and
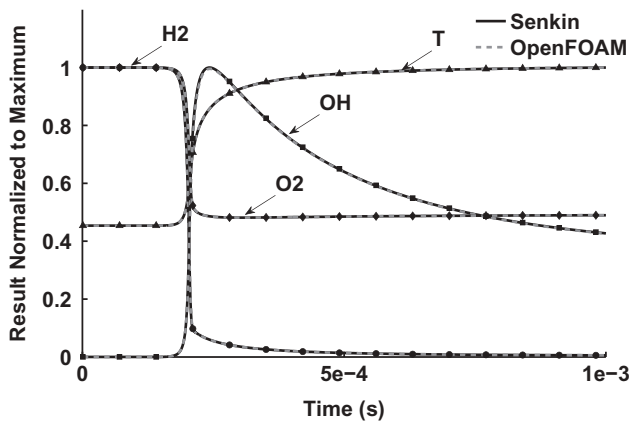
Figure 18 Comparison of temperature and species evolution of a homogeneous mixture at constant pressure and constant enthalpy conditions using OpenFOAM and SENKIN codes. Results are normalized to their maximum values, i.e., $T/T_{\max}$, $X_{H_2}/\left(X_{H_2}\right)_{\max}$, $X_{O_2}/\left(X_{O_2}\right)_{\max}$, and $X_{OH}/\left(X_{OH}\right)_{\max}$.
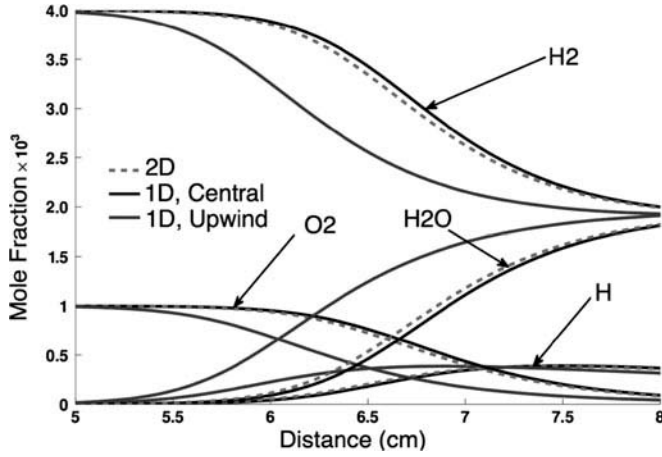
Figure 19 Variation of species mole fractions in a one-dimensional reactor at constant $T = 980$ K and $p = 1$ atm, with inflow conditions of $v = 2$ m/s, $X_{H_2} = 0.004$, $X_{O_2} = 0.001$, and $X_{N_2} = 0.995$.

$X_{N_2} = 0.995$, with a constant temperature of 980 K. Pressure was treated as constant at 1 atmosphere in the Sandia code, while the OpenFOAM's PISO method with a far-field pressure node introduced a small pressure departure of the order of 10^{-3} Pa throughout the computational domain. For the above highly diluted case, a 1D mesh was constructed for the OpenFOAM case, with grid spacing in the axial direction of 100 µm.

Although the species concentrations are small, for the highly reactive hydrogen-oxygen mixture with large species gradients are sensitive to the order of discretization of governing equations. Specifically, for a well resolved case, implementation of a central differencing scheme in Sandia 1D premix code is found to yield better agreement with the second-order accurate FVM in OpenFOAM, as shown in Figure 19. As seen in this figure, the default upwind discretization yields a markedly different species profile.

## Counterflow Flame Structure and Extinction Limits

To verify that the OpenFOAM solver could sufficiently simulate counter-flow flame structure and extinction limits, a direct comparison study was performed in comparison to the solution of quasi 1D governing equations using Smooke's code (Smooke et al., 1991) and Sandia Oppdif Code (Lutz et al., 1997). It is worth noting that the default discretization of species and energy equations of Sandia and Smooke's codes is upwind for advection terms and central-differencing for diffusion terms. For the same inflow boundary conditions of a diluted hydrogen-air non-premixed flame, these two codes resulted in a 4 K difference in the peak flame temperature for a moderately strained flame with a similar grid resolution, which we were unable to explain. However, implementation of a central difference scheme for the advection terms in Smooke's code resulted in a 12 K peak temperature difference. Thus, we believe that the observed peak temperature deviation of 10–15 K between OpenFoam and quasi 1D solvers is likely to be due to numerics. Such temperature differences are expected to influence global flame property comparisons.

Even though it is not the main focus of the present article, the ability to not only predict the flame structure but also predict the extinction limits using the OpenFOAM solver

was explored using the Seshadri type flow configuration with a plug-flow velocity profile at the inlets, as shown in Figure 2a. In this study, the computation domain considered was a smaller 13.5 mm by 13.5 mm axisymmetric domain. The non-premixed inflow of fuel and oxidizer streams consisted of diluted hydrogen ($X_{H_2} = 0.16$, $X_{N_2} = 0.84$) versus air ($X_{O_2} = 0.21$, $X_{N_2} = 0.79$). The temperature of both inflow streams were assumed to be at 300 K. The outflow boundary condition used a far-field condition for pressure and Neumann condition for all other quantities. The opposed stream flow velocities were gradually increased and convergence was confirmed at strain rates ranging from 200 to 450 s^{-1} (quasi 1D solutions predict flame extinction at about 480 s^{-1}). For consistency, both simulations used mixture averaged diffusion for species transport, a detailed hydrogen kinetic model extracted from JetSurf2.0 (Wang et al., 2011), and the same uniform grid resolution of 15 μm. A comparison of the predicted flame structure for a local strain rate of 365 s^{-1} is shown in Figure 20, with comparison to the Smooke's quasi 1D code solution. For the case shown, the temperature difference is within 2 K. Figure 21 shows a comparison of the predicted peak flame temperature versus local strain rate, for the same axisymmetric case with plug-flow boundary conditions (Seshadri type burner) using OpenFOAM solver and Smooke's quasi 1D code (Smooke et al., 1991). Numerical error effects in OpenFOAM and the origin of uncertainties shown in Figure 21 are discussed next.

Grid Resolution Effects

Numerical error and grid dependence effects were analyzed in order to remove the possibility that the general trends highlighted are due to numerical sources. A systematic grid refinement study was examined to determine the grid independence for the OpenFOAM cases. Since the discretization scheme used here was second-order accurate, the observed order of accuracy for a response quantity should be close to 2.0. For a reacting case, three consecutive grid refinements yielded observed order of accuracies of 1.84, 1.78, and 1.67 for strain rate, maximum temperature, and H-atom concentrations, respectively. This confirms that the grid choices used in this article are within the asymptotic range and grid independent. These observed order of accuracies were greater than 1.5, which allowed
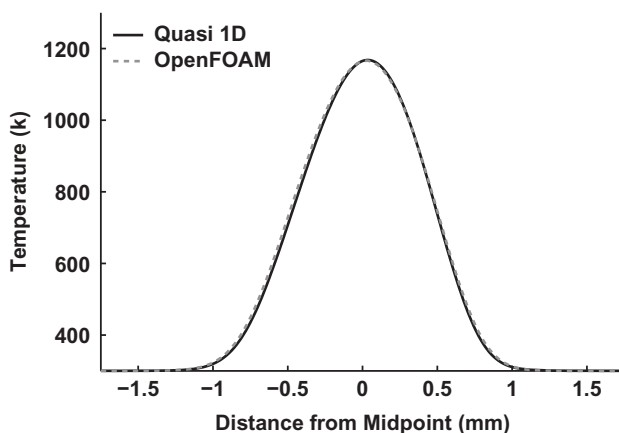
Figure 20 Comparison of the flame temperature profiles predicted using OpenFOAM and quasi one-dimensional codes, for strain rates of $a = 375\, s^{-1}$.
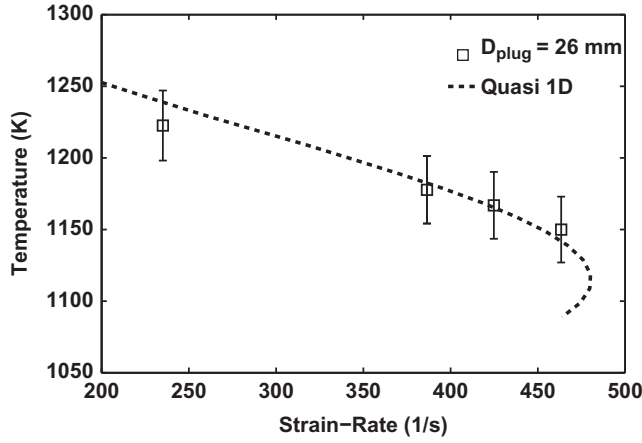
Figure 21 Prediction of maximum flame temperature variation with increasing flow strain rate of a diluted non-premixed hydrogen vs. air flame, using both OpenFOAM and quasi one-dimensional simulations.

a factor of safety of 1.5 in the calculation of a grid convergence index (GCI) using Roache's method and Richardson extrapolation (see Roy and Oberkampf, 2010). This resulted in error estimates of less than 2% for $\Delta x = 15\,\mu$m, for the peak temperature in the counter-flow flame simulations that were used to verify the OpenFOAM solver. When the 2% error applied to temperature obtained from the OpenFOAM solver, Figure 21 shows a predicted flame temperature uncertainty versus local flow strain rate.